Enzymology:

Human 60-kDa Lysophospholipase Contains an N-terminal l-Asparaginase Domain That Is Allosterically Regulated by l-Asparagine

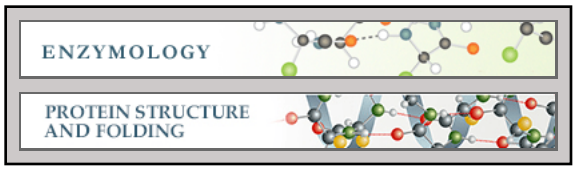

Christos S. Karamitros and Manfred Konrad

J. Biol. Chem. 2014, 289:12962-12975.
doi: 10.1074/jbc.M113.545038 originally published online March 22, 2014

THE JOURNAL OF BIOLOGICAL CHEMISTRY VOL. 289, NO. 19, pp. 12962–12975, May 9, 2014

Human 60-kDa Lysophospholipase Contains an N-terminal L-Asparaginase Domain That Is Allosterically Regulated by L-Asparagine*[S]

Received for publication, December 20, 2013, and in revised form, March 2, 2014 Published, JBC Papers in Press, March 22, 2014, DOI 10.1074/jbc.M113.545038

Christos S. Karamitros and Manfred Konrad[1]

From the Enzyme Biochemistry Group, Max Planck Institute for Biophysical Chemistry, Göttingen D-37077, Germany

Background: The 60-kDa human lysophospholipase comprises an N-terminal domain with predicted, yet uncharacterized L-asparaginase activity and a C-terminal ankyrin repeat-like domain.
Results: The N-terminal domain, termed hASNase1, was identified as a functional structural unit possessing catalytic activity.
Conclusion: hASNase1 is an allosterically regulated bacterial-type cytoplasmic L-asparaginase.
Significance: Domains of multifunctional human proteins harbor homologs of prokaryotic enzymes displaying similar structural and kinetic features.

The structural and functional characterization of human enzymes that are of potential medical and therapeutic interest is of prime significance for translational research. One of the most notable examples of a therapeutic enzyme is L-asparaginase, which has been established as an antileukemic protein drug for more than four decades. Up until now, only bacterial enzymes have been used in therapy despite a plethora of undesired side effects mainly attributed to the bacterial origins of these enzymes. Therefore, the replacement of the currently approved bacterial drugs by human homologs aiming at the elimination of adverse effects is of great importance. Recently, we structurally and biochemically characterized the enzyme human L-asparaginase 3 (hASNase3), which possesses L-asparaginase activity and belongs to the N-terminal nucleophile superfamily of enzymes. Inspired by the necessity for the development of a protein drug of human origin, in the present study, we focused on the characterization of another human L-asparaginase, termed hASNase1. This bacterial-type cytoplasmic L-asparaginase resides in the N-terminal subdomain of an overall 573-residue protein previously reported to function as a lysophospholipase. Our kinetic, mutagenesis, structural modeling, and fluorescence labeling data highlight allosteric features of hASNase1 that are similar to those of its *Escherichia coli* homolog, *Ec*ASNase1. Differential scanning fluorometry and urea denaturation experiments demonstrate the impact of particular mutations on the structural and functional integrity of the L-asparaginase domain and provide a direct comparison of sites critical for the conformational stability of the human and *E. coli* enzymes.

L-Asparaginases (EC 3.5.1.1; L-asparagine amidohydrolase; L-ASNase[2]) are enzymes that primarily catalyze the conversion of L-asparagine (L-Asn) to L-aspartic acid (L-Asp) and ammonia, although some of them are able to also hydrolyze L-glutamine (L-Gln) to L-glutamic acid (L-Glu) and ammonia. These enzymes are present in bacteria to mammals and play pivotal roles in amino acid metabolism (1, 2). Enzymes with L-asparaginase activity can be generally classified into two evolutionary distinct families: the bacterial-type and the plant-type L-asparaginases, which are characterized by different structural and biochemical features (3, 4). The bacterial-type enzymes have been further grouped into type I and type II depending on their cellular localization. Type I includes cytosolic enzymes that exhibit low affinity (millimolar K_m) for L-Asn, whereas type II enzymes are localized in the periplasm and show considerably higher affinity (micromolar K_m) for L-Asn (5). These enzymes have been studied extensively over the last 40 years mainly because two of the type II isoforms (L-ASNases from *Escherichia coli* and *Erwinia chrysanthemi* encoded by the *ansB* genes) serve as therapeutics for the treatment of acute lymphoblastic leukemia (6–8). Conversely, the less studied plant-type L-asparaginases belong to the so-called N-terminal nucleophile (Ntn) hydrolases, which were defined as a new protein structural family in 1995 (9). A major characteristic of this Ntn hydrolase superfamily is a post-translational processing step that generates the active enzyme. The enzymes are expressed as inactive precursors that undergo a slow intramolecular autoproteolytic cleavage reaction at a specific site resulting in two tightly associated subunits, α and β, also called protomers. The catalytic residue acting as the nucleophile is exposed at the very N terminus of the newly generated β-subunit, which remains complexed with the α-subunit during catalysis (10–12). A well characterized mammalian member of the Ntn nucleophile hydrolase superfamily is the human lysosomal aspartylgluco-

* This work was supported by the Max Planck Society (to C. S. K. and M. K.) and the Göttingen Graduate School for Neurosciences, Biophysics, and Molecular Biosciences (to C. S. K.).
[S] This article contains a supplemental table.
[1] To whom correspondence should be addressed. Tel.: 49-551-2011706; Fax: 49-551-2011074; E-mail: mkonrad@gwdg.de.
[2] The abbreviations used are: L-ASNase, L-asparaginase; hASNase1, human L-asparaginase 1; *Ec*ASNase1, *E. coli* L-asparaginase 1; *Ph*ASNase1, *P. horikoshii* L-asparaginase 1; *Rn*ASNase1, *R. norvegicus* L-asparaginase 1; *Sc*ASNase1, *S. cerevisiae* L-asparaginase 1; *ansA*, gene name for cytoplasmic bacterial L-asparaginases; *ansB*, gene name for periplasmic bacterial L-asparaginases; Ntn, N-terminal nucleophile; palmitoyl-lysoPC, 1-palmitoyl-*sn*-glycero-3-phosphocholine; lysoPI, lysophosphatidylinositol; ADIFAB, acrylodated intestinal fatty acid-binding protein; SUMO, small ubiquitin modifier; Ni-NTA, nickel-nitrilotriacetic acid; CAPSO, 3-(cyclohexylamino)-2-hydroxy-1-propanesulfonic acid.

saminidase, which catalyzes the hydrolysis of glucosylated L-Asn molecules generated during proteolytic breakdown of glycoproteins (13, 14). The human genome encodes another enzyme of this Ntn hydrolase family, variably termed human asparaginase-like protein 1 (15), glial asparaginase (16), CRASH (17), or hASNase3 because its high homology with *E. coli* L-ASNase3 (encoded by the *iaaA* gene) (18). Crystal structures of the wild-type form and of a circular permutant version of hASNase3 have been reported recently (19–22).

The two aforementioned human enzymes and some of their microbial and plant homologs have been characterized as representatives of the Ntn hydrolase superfamily. In contrast, little is known about bacterial-type L-asparaginases expressed in mammalian tissues. An interesting example of such an enzyme is the 60-kDa lysophospholipase first isolated from rat liver (23). This enzyme comprises two domains: an N-terminal domain that is homologous to the *E. coli* cytoplasmic-type I L-asparaginase (*Ec*ASNase1; encoded by the *ansA* gene) and a C-terminal ankyrin repeat-like domain. This 60-kDa lysophospholipase from rat liver was shown to exhibit three distinct enzymatic activities (lysophospholipase, L-asparaginase, and platelet-activating factor acetylhydrolase) (23); however, no further studies have been reported on this protein, and little is known about its human homolog. In fact, the human 60-kDa lysophospholipase is a poorly characterized protein that shows 79% overall amino acid sequence identity with its rat homolog. In addition, although it has been demonstrated (24) that the protein holds lysophospholipase activity *in vitro* and plays a key role in cell proliferation and regulation of membrane channels, there are no supporting data to assign L-asparaginase activity to this human two-domain protein.

The present study focuses on the bacterial expression, purification, and biochemical characterization of the N-terminally located L-asparaginase domain (residues 1–369) of the 60-kDa (573-residue) human lysophospholipase. Because of high sequence similarity of this domain with *Ec*ASNase1 (47% identity), we designate it as hASNase1. Lysophospholipase activity was detected neither for the hASNase1 enzyme nor for the bacterial homolog. We show that the purified enzyme exhibits characteristics similar to those of bacterial type I L-asparaginase. Our kinetic and mutagenesis studies on hASNase1 unveil strong positive allosteric modulation as a function of L-Asn concentration through the action of a second L-Asn binding site, which we probed by cysteine-specific fluorescence labeling of the allosteric site. These results are in line with a previous crystallographic and mechanistic study on the *E. coli* cytoplasmic homolog demonstrating L-Asn-dependent allosteric regulation of the bacterial enzyme *in vitro* (25). Interestingly, we observed a substrate-inducing effect on the oligomeric state of hASNase1; however, the predominant state of the enzyme at assay conditions is monomeric. Our thermodynamic analysis of hASNase1 suggests conformational features and stability distinct from its *E. coli* counterpart. By mutational analysis, we highlight critical residues located at its putative allosteric and catalytic sites.

EXPERIMENTAL PROCEDURES

Materials—Yeast extract, peptone from casein, NaCl, Nessler's reagent, urea, SYPRO Orange, L-asparagine, L-glutamine, L-aspartic acid, glutamate dehydrogenase, α-ketoglutarate, NADH, synthetic 1-palmitoyl-*sn*-glycero-3-phosphocholine (palmitoyl-lysoPC), lysophosphatidylinositol (lysoPI) from *Glycine max* (highly polyunsaturated soybean oil; mixture of different fatty acids and enriched with stearic and palmitic acids), phospholipase A_2 from bovine pancreas, L-α-phosphatidylcholine from soybean (mixture of different fatty acids), and palmitic acid were purchased from Sigma-Aldrich-Fluka. The acrylodated intestinal fatty acid-binding protein (ADIFAB) assay kit was obtained from FFA Sciences (San Diego, CA). Dialysis membranes and Coomassie Brilliant Blue G-250 (Bradford reagent) were from Roth (Karlsruhe, Germany). Slide-A-Lyzer was from Pierce. Oligonucleotides were synthesized by IBA GmbH (Goettingen, Germany). Restriction enzymes and T4 DNA ligase were obtained from New England Biolabs (Ipswich, MA). KAPA HiFi polymerase and all PCR reagents were from PeqLab (Erlangen, Germany). Gel extraction and PCR product purification kits as well as nickel-agarose (Ni-NTA) for protein purification were purchased from Macherey Nagel (Düren, Germany). Plasmid purification kits were from Fermentas (Thermo Fisher Scientific, Germany). Genomic DNA preparation kits were from Qiagen (Hilden, Germany).

Cloning of hASNase1, EcASNase1, and Chaperonin 10—The cDNA region coding for the N-terminal domain (termed hASNase1) of the full-length 60-kDa human lysophospholipase was PCR-amplified using as template a cDNA clone of the *ASPG* gene (human L-asparaginase homolog, NCBI Reference Sequence NM_001080464; GenBank™ accession number BC035836) isolated from female ovarian tissue (Source Bioscience, UK). Four different C-terminal truncation constructs of hASNase1 were generated and subsequently tested for solubility and enzymatic activity as described in the following sections. NdeI and BamHI sites, respectively, were incorporated in the 5′-ends of the amplifying oligonucleotides (primers are listed in the supplemental table). The PCR mixture in a 50-μl final volume consisted of 50 ng of template plasmid DNA, oligonucleotide mixture (10 pmol each), KAPA high fidelity buffer, dNTPs (0.2 mM each), and 1 unit of KAPA HiFi DNA polymerase. The PCR fragment was gel-purified and subjected to additional overlap extension PCRs aiming at the elimination by silent mutation of an internal BamHI restriction site (nucleotide sequence position 740) whose presence would limit the unique cleavage at the 3′-end. The final PCR product was digested with NdeI and BamHI and ultimately ligated overnight at 16 °C into the pET14b-SUMO vector (10) using T4 DNA ligase. The ligation mixture was used to transform DH5α *E. coli* cells. Plasmid DNA isolated from single colonies was digested with NdeI and BamHI to identify positive clones, some of which were sequence-verified. The final constructs include an N-terminal six-histidine tag (His_6) followed by the small ubiquitin modifier (SUMO; Smt3p protein from yeast; 101 residues; molecular mass, 11.2 kDa) tag, which has been shown to improve heterologous protein solubility and stability (26). For bacterial expression, the *E. coli* BL21(DE3) pLysS strain was transformed with

each of the four hASNase1 constructs. Expression vectors for *Ec*ASNase1 and Chaperonin 10 (GroES; encoded by the *Cpn10* gene) were constructed analogously.

Mutagenesis of hASNase1 and EcASNase1—All hASNase1 single site mutants (T19A, T116A, T187S, T187A E266R, E266S, and C299S) and *Ec*ASNase1 mutants (R240E and C273S) were generated by applying the QuikChange methodology (Stratagene) using as templates the cloned wild-type genes and KAPA HiFi DNA polymerase. Mutants T187S and T187A were generated in a single PCR using the same pair of primers by making use of the wobble-type oligonucleotides (G/T) at the first nucleotide of the T187 codon (ACC). Mutants E266R and E266S were constructed in a similar way (the primers are listed in the supplemental table). Site-specific mutations were confirmed by sequencing the entire coding regions (Seqlab, Goettingen, Germany). All hASNase1 mutants were expressed and purified following the protocol described below for the wild-type enzyme.

Protein Expression and Purification of hASNase1, EcASNase1, and GroES—*E. coli* BL21(DE3) pLysS cells containing the hASNase1 plasmid were cultured overnight at 37 °C in LB medium supplemented with 200 μg/ml ampicillin and 35 μg/ml chloramphenicol. A fraction of this culture (dilution 1:100) was used to inoculate fresh 2× YT medium (1% yeast extract, 1.6% Tryptone, 0.5% NaCl) supplemented with 200 μg/ml ampicillin and 35 μg/ml chloramphenicol. When the bacterial culture reached an A_{600} of ~0.5–0.7, its temperature was lowered to 22 °C, and protein expression was induced by adding isopropyl 1-thio-β-D-galactopyranoside to a final concentration of 0.25 mM. After incubation at 16 °C for 18 h, the cells were centrifuged at 4,000 × *g* for 30 min, resuspended in Ni-NTA-agarose affinity matrix binding buffer A (50 mM Na_2HPO_4, 0.3 M NaCl, 10 mM imidazole, 2% glycerol, 1 mM PMSF, pH 8.0), and ultimately lysed by sonication. The cell lysate was centrifuged at 17,200 × *g* for 45 min, and to the cleared supernatant was added a fraction (1:10 dilution) of 10× ATP buffer B (50 mM Na_2HPO_4, 0.3 M NaCl, 100 mM ATP, 200 mM $MgCl_2$, 500 mM KCl, pH 8.0). The combined mixture was incubated in a 37 °C water bath for 15 min, mixed with pre-equilibrated Ni-NTA-agarose beads, and incubated at 4 °C for 3 h under rotation. Subsequently, the mixture was transferred to a 12-ml polypropylene column and dried by gravity. To remove unspecifically adsorbed material, the nickel resin was first washed with 25 bed volumes of washing buffer C (50 mM Na_2HPO_4, 0.5 M NaCl, 20 mM imidazole, 2% glycerol, pH 8.0). The resin was then mixed with a 10-fold diluted buffer B supplemented with GroES at a final concentration of 50 μM. The mixture was incubated at 4 °C for 2 h under rotation, dried by gravity, and then further washed with 10 bed volumes of buffer B without GroES. Finally, the bound His_6-SUMO-hASNase1 protein was eluted from the column by applying 300 mM imidazole in buffer A, and fractions were collected dropwise and tested for L-asparaginase activity. All purification steps were performed at 4 °C. The fractions that contained active hASNase1 were mixed, buffer was exchanged against buffer D (20 mM Tris-Cl, 5% glycerol, pH 8) using a PD-10 column (GE Healthcare), and then the sample was subjected to DEAE Sephacel anion exchange chromatography. Elution was performed by applying an NaCl gradient (0–250 mM) in buffer D. Fractions were analyzed by SDS-PAGE, those containing >90% pure hASNase1 were pooled, and buffer was exchanged against buffer E (50 mM Tris-Cl, 100 mM NaCl, pH 8). The protein was incubated with yeast SUMO protease (molar ratio of protease: protein, ~1:100) at 4 °C overnight (alternatively 2 h at 30 °C) to cleave the N-terminal His_6-SUMO tag. In the last purification step, the protein was subjected to size exclusion chromatography by passing it through a Superdex 200 column (size, 30 × 1 cm; GE Healthcare) to remove the cleaved tag and remaining impurities. Protein purity was evaluated by SDS-PAGE and was estimated to exceed 95%. The protein sample was aliquoted, mixed with 25% glycerol, and stored at −20 °C at a final concentration of 2 mg/ml until use. The aforementioned purification protocol was followed for the purification of wild-type hASNase1 as well as for all mutants described in this study. The final average yield of the purified human enzymes was ~ 0.3 mg/liter of 2× YT medium. *Ec*ASNase1 and GroES were purified following the protocol described for hASNase1 excluding the washing steps with ATP and GroES as well as the intermediate anion exchange treatment. *Ec*ASNase1 and GroES purifications yielded ~10 and 2 mg/liter of 2× YT medium, respectively. Protein quantification was performed by using the Bradford method (27) and by the calculated molar absorption coefficient of each enzyme (23,295 M^{-1} cm^{-1} for hASNase1; 26,360 M^{-1} cm^{-1} for *Ec*ASNase1; 1,490 M^{-1} cm^{-1} for GroES) at 280 nm based on the amino acid sequence (28). The two quantification methods showed less than 10% difference, and ultimately the values were averaged.

L-Asparaginase and Lysophospholipase Activity Assays—We applied two different methods for monitoring L-asparaginase activity: a single step discontinuous method and a two-step continuous assay for real time measurements of the enzymatic activity. The discontinuous method, the so-called Nesslerization procedure that quantifies ammonia liberated upon deamidation of L-asparagine, has been described previously (29). The continuous assay, which monitors the NADH-dependent conversion of α-ketoglutarate plus ammonia to glutamate in a glutamate dehydrogenase-coupled reaction (30), was applied for the kinetic characterization of the enzymes using a Uvikon 943 double beam UV/visible spectrophotometer. All enzymes used for the activity measurements and the kinetic experiments were free of the His_6-SUMO tag, which was removed during the last size exclusion chromatographic step (see above). For steady-state kinetic analysis, L-Asn concentrations in the range of $0-10K_m$ were tested in a final volume of 1 ml of 50 mM Tris-Cl, 100 mM NaCl, pH 8 at 37 °C. The final enzyme concentration was ~0.5 μM (20 μg in 1 ml). The obtained V/E (velocity/total enzyme concentration) values were plotted against the respective substrate concentrations. Kinetic constants $S_{0.5}$ and k_{cat} were calculated from the resulting plots by non-linear regression using the Hill equation (Equation 1) and analyzed by the SoftZymics software (Igor Pro, Wavemetrics).

$$V = \frac{V_{max}[S]^n}{[S]_{0.5}^n + [S]^n} \quad \text{(Eq. 1)}$$

Here, V is the initial velocity of the enzymatic reaction, V_{max} is the maximal velocity, $[S]$ is the substrate concentration, $[S_{0.5}]$ is

the substrate concentration that yields half-maximal velocity, and n is the Hill coefficient.

Potential lysophospholipase activity of hASNase1 was tested using a continuous fluorescence assay as described previously (31). Briefly, this assay detects free fatty acid molecules, which are released upon hydrolysis of lysophospholipids by lysophospholipases; free fatty acid then is complexed with the intestinal fatty acid-binding protein conjugated with the fluorescent probe acrylodan, commercially known as a free fatty acid indicator and abbreviated as ADIFAB. Free fatty acid binding to ADIFAB induces a fluorescence signal decrease due to changes of the position of the acrylodan fluorophore, which is located close to the free fatty acid binding pocket of intestinal fatty acid-binding protein. In the present study, we tested palmitoyl-lysoPC and lysoPI as candidate substrates of hASNase1. The assay was performed in a quartz cuvette according to the manufacturer's instructions using final concentrations of 100 μM for each substrate, 1 μM ADIFAB, and 1.8 μM enzyme (15 μg) in 200 μl of 50 mM HEPES, 140 mM NaCl, 5 mM KCl, 1 mM Na_2HPO_4, pH 7.5. Fluorescence intensity was recorded continuously for 10 min at 25 °C using a Jasco FP 8300 spectrofluorometer in the high sensitivity mode (excitation at 386 nm and emission at 432 nm with 2.5-nm bandwidths). The assay was initially standardized by testing the fluorescence signal decrease upon binding of palmitic acid (one of the expected products of substrate hydrolysis; lysoPI contains a mixture of fatty acid derivatives; see "Materials") with the ADIFAB sensor protein as well as by measuring the activity of phospholipase A_2 against L-α-phosphatidylcholine (also provided as a mixture of different fatty acid derivatives). Both hASNase1 and *Ec*ASNase1 were tested for lysophospholipase activity.

Homology Modeling of hASNase1—A homology model of the N-terminal L-asparaginase domain of the 60-kDa human lysophospholipase based on the recently determined structure of the homologous *Ec*ASNase1 enzyme (25) was obtained from the protein structure prediction service Phyre (32) (Job code 77beadcf4ff84dfc, Fold Library ID c2p2dA, identity of 47%, estimated precision of 100%). The resulting hASNase1 structure was overlaid on the *Ec*ASNase1 crystal structure (Protein Data Bank code 2HIM) using PyMOL (33). The putative allosteric and catalytic sites of hASNase1 were analyzed for the presence of critical residues previously identified in *Ec*ASNase1.

Probing the Putative Allosteric Site of hASNase1 by Fluorescence Labeling of Cys^{299}—Cysteine residue Cys^{299} of the catalytically inactive T19A mutant of hASNase1 was labeled using the compound Atto 465-maleimide as a fluorescent dye (Sigma-Aldrich). Maleimides show excellent reactivity with thiol groups, and therefore, they can serve as site-specific labeling probes in cases where reduced cysteines are available. Labeling was done in the following way. Highly purified enzyme (>95% pure as determined by SDS-PAGE) in 20 mM Tris-Cl, 100 mM NaCl, pH 7.2 was mixed under stirring with a 10-fold molar excess of the dye (dissolved in DMSO). The final concentrations in the reaction mixture (0.5 ml) were 20 μM enzyme and 200 μM dye. The mixture was incubated at 22 °C for 2 h in the dark, and subsequently 1 mM of glutathione (GSH) was added to remove excess thiol-reactive dye. The labeled enzyme mixture was dialyzed against 50 mM Tris-Cl, 100 mM NaCl, pH 8. The labeling of the enzyme was confirmed by SDS-PAGE analysis applying 5 μg each of unlabeled enzyme and of the final enzyme-dye conjugate because it has been shown (34) that labeled proteins migrate more slowly than unlabeled species.

For measuring interactions of hASNase1 with L-Asn, L-Asn in the concentration range of 0.1–40 mM was incubated with labeled enzyme (1.5 μM final concentration) in a final volume of 100 μl. The samples were left for 2 h on ice to equilibrate. Fluorescence intensity was recorded using a Jasco FP 8300 spectrofluorometer in the high sensitivity mode (excitation at 463 nm and emission at 508 nm with 2.5-nm bandwidths). All measurements were done in triplicate. Because hASNase1 contains overall 6 cysteines, the mutant C299S was also labeled and served as a negative control (background fluorescence) for signal changes upon L-Asn binding. The resulting saturation binding curve was fitted using SoftZymics software (Igor Pro, Wavemetrics) according to Equation 2,

$$F = F_0 - \frac{F_{max}[S]}{K_d + [S]} \quad \text{(Eq. 2)}$$

where F is the fluorescence intensity, F_0 is the fluorescence intensity at zero concentration of ligand, F_{max} is the plateau fluorescence intensity, K_d is the dissociation constant, and $[S]$ is the ligand concentration.

Thermodynamic Characterization of hASNase1 Conformational Stability—The conformational stability of hASNase1 and *Ec*ASNase1 was studied by monitoring changes in intrinsic fluorescence of the stepwise urea-denatured proteins (35, 36). The final urea concentrations ranged from 0.5 to 8 M using a stock solution of 10 M urea dissolved in 50 mM Tris-Cl, 100 mM NaCl, pH 8. The final concentration of the enzymes was adjusted to 50 μg/ml (~1.25 μM for both enzymes) in a final volume of 100 μl. The two tryptophan residues of hASNase1 (Trp^{93} and Trp^{150}) exhibited intrinsic fluorescence upon excitation at 295 nm (this wavelength was chosen to reduce excitation of tyrosines), showing an emission maximum at 343 nm. The same excitation and emission maxima were obtained for *Ec*ASNase1 containing a single tryptophan residue (Trp^{68}). Before measurements, equilibrium of the unfolding reactions was confirmed by monitoring the fluorescence signals at different time points until no further change was observed. Data were analyzed assuming a two-state model for reversible protein unfolding. Isothermal urea-induced unfolding experiments were carried out at 10, 15, 20, 25, 30, 35, and 40 °C. For each temperature, data analysis using the linear extrapolation method (37) yielded three parameters: (i) the difference of Gibbs free energy between the native and the unfolded state of the protein (ΔG_{H2O}); (ii) the dependence of ΔG_{H2O} on denaturant concentration (parameter m, which is the slope of the equation $\Delta G = \Delta G_{H2O} - m[\text{urea}]$), which can be thought of as a measure for the sensitivity of the protein toward the unfolding agent; and (iii) the concentration of urea at which the protein is half-unfolded ($C_{1/2}$). Subsequently, the calculated ΔG_{H2O} values (free energy change at zero concentration of urea) resulting from each temperature were fitted to the Gibbs-Helmholtz equation (Equation 3) (37) as a function of temperature to obtain the ΔC_p values. T_m and ΔH_m values as fitting parameters were

calculated from temperature-induced denaturation experiments (range, 15–85 °C) following the intrinsic tryptophan fluorescence changes of protein similar to urea experiments.

$$\Delta G(T) = \Delta H_m(1 - T/T_m) - \Delta C_p[(T_m - T) + T \ln(T/T_m)] \quad \text{(Eq. 3)}$$

$\Delta G(T)$ is the Gibbs free energy difference between the folded and unfolded state at temperature T, T_m is the melting temperature, ΔH_m is the enthalpy difference at T_m, and ΔC_p the heat capacity difference of the folded and unfolded states at constant pressure.

Thermal Stability Determination of Wild-type and Mutant hASNase1 Enzymes by Differential Scanning Fluorometry—The effect of point mutations on thermal stability of hASNase1 was studied by applying differential scanning fluorometry techniques (38, 39). Enzyme samples were dialyzed (Slide-A-Lyzer, Pierce; 10,000 molecular weight cutoff) against 50 mM Tris-Cl, 0.1 NaCl, pH 8 to remove glycerol and subsequently mixed with SYPRO Orange (Sigma-Aldrich) in a final volume of 20 μl. The final concentrations of the enzyme and the dye were 2 μM and 10% (v/v), respectively; the DMSO stock solution of the dye (5,000×) was prediluted in H_2O, giving a 100× solution, from which aliquots were used according to the experimental needs. The samples were mixed in a 96-well plate suitable for real time PCR measurements, centrifuged at 500 rpm for 30 s, and finally sealed with heat-resistant membranes (Microseal B adhesive sealer) to prevent evaporation. The enzyme melting experiments were performed using a CFX96 real time PCR machine (Bio-Rad) with the following settings: 2-min prewarming step at 30 °C and subsequent gradient between 31 and 95 °C with 1 °C/min increments. SYPRO Orange fluorescence was monitored using the filters provided with the machine: FAM (492 nm) for excitation and ROX (610 nm) for emission. Data were exported as an Excel-based worksheet and further analyzed by Igor Pro (Wavemetrics). Melting temperatures (T_m) were obtained by plotting the first derivative d(AFU)/dT (where AFU represents arbitrary fluorescence units) of the raw data as a function of temperature increase (40).

Effects of pH, Divalent Metal Ions, and DTT on Enzyme Activity and Stability—Effects of pH on enzymatic activity and stability were assessed in a broad range of pH values using several buffers: sodium acetate (pH 3–5), sodium phosphate (pH 6–7), Tris-Cl (pH 7–8.5), and CAPSO (pH 9–10), all at 50 mM concentration in the presence of 100 mM NaCl. For the investigation of the pH effect on the activity of the enzyme, ~50 μg of enzyme were assayed in a final volume of 1 ml at saturating substrate concentration (20 mM L-Asn) applying the Nesslerization method. The discontinuous method was preferred to the NADH-dependent continuous assay because the different pH values could influence the activity of the auxiliary glutamate dehydrogenase enzyme, resulting in unforeseeable artifacts. The stability of hASNase1 under various pH conditions was studied by incubating the enzyme (at 0.1 mg/ml final concentration) in several buffers for 12 h at 4 °C. Aliquots of these mixtures were assayed for residual L-asparaginase activity by Nesslerization using as standard buffer the one at which the enzyme showed the highest activity based on the previous activity analysis. To study metal ion effects, purified hASNase1 (0.1 mg/ml) was preincubated with a final concentration of 1 mM for each of several divalent metal ions, EDTA, and DTT for 3 h at 4 °C. Subsequently, aliquots were tested for residual activity by the Nesslerization method.

RESULTS

Expression and Purification of the hASNase1 Domain—Four different C-terminal truncations (numbered 1, 2, 3, and 4; see Fig. 2*A*) of full-length human lysophospholipase (gene code *ASPG*; asparaginase homolog) were designed based on sequence alignments of the N-terminal putative L-asparaginase domain and different procaryotic (*E. coli*, *Ec*ASNase1, and *Pyrococcus horikoshii*, *Ph*ASNase1) and eucaryotic (*Rattus norvegicus*, *Rn*ASNase1, and *Saccharomyces cerevisiae*, *Sc*ASNase1) cytoplasmic L-asparaginases (Fig. 1). All four constructs were tested for protein expression in *E. coli* and solubility under a spectrum of different conditions (culture medium, *E. coli* strain, isopropyl 1-thio-β-D-galactopyranoside concentration, and temperature). Interestingly, truncation 3, which appears to fit best to the bacterial cytoplasmic enzymes according to the amino acid sequence comparison, was not soluble, and trials to purify the enzyme under denaturation/renaturation conditions (unfolding by up to 8 M urea and refolding by dialysis) ultimately resulted in a catalytically inactive protein. Similarly, truncations 1 and 2 failed to produce soluble, active hASNase1. In contrast, truncation 4 (369 amino acid residues), containing 5 additional amino acids (VEERR) downstream of truncation 3, produced the protein in soluble form (Fig. 2*B*), and most importantly, the protein purified under native conditions exhibited L-asparaginase activity.

However, when the protein purity was analyzed by SDS-PAGE after the last gel filtration step (see "Experimental Procedures"), a prominent band with an apparent molecular mass of ~60 kDa and an estimated stoichiometric 1:1 ratio to the hASNase1 band was constantly observed (Fig. 3). Multiple attempts to remove this associated protein species by altering standard purification protocols were unsuccessful. This prompted us to analyze this protein band by mass spectrometry by which it was finally identified as the endogenous *E. coli* chaperone GroEL. Indeed, contamination by co-purified chaperones can be a hurdle in recombinant protein expression and purification setups (41). Although it has been described previously (42) that incubation of the crude cell extract with 10 mM ATP at 37 °C and washing of the affinity column with an ATP-containing buffer facilitate the removal of GroEL, this approach did not prove beneficial in our case. Moreover, attempts to use an engineered *E. coli* strain (43) (a kind gift from Prof. Ulrich Hartl's laboratory, Max Planck Institute for Biochemistry, Munich, Germany) carrying the GroEL/ES operon under an arabinose-inducible promoter, which allows tuned regulation of the expression levels of these chaperones, failed to produce the hASNase1 protein (data not shown). Ultimately, we managed to remove the co-purified chaperone by including in the washing buffer the natural binding partner of this protein, GroES, at ~10-fold excess over GroEL (44). It appears reasonable to assume that the presence of ATP-Mg^{2+}-GroES weakened the binding between GroEL and hASNase1, thus facilitat-

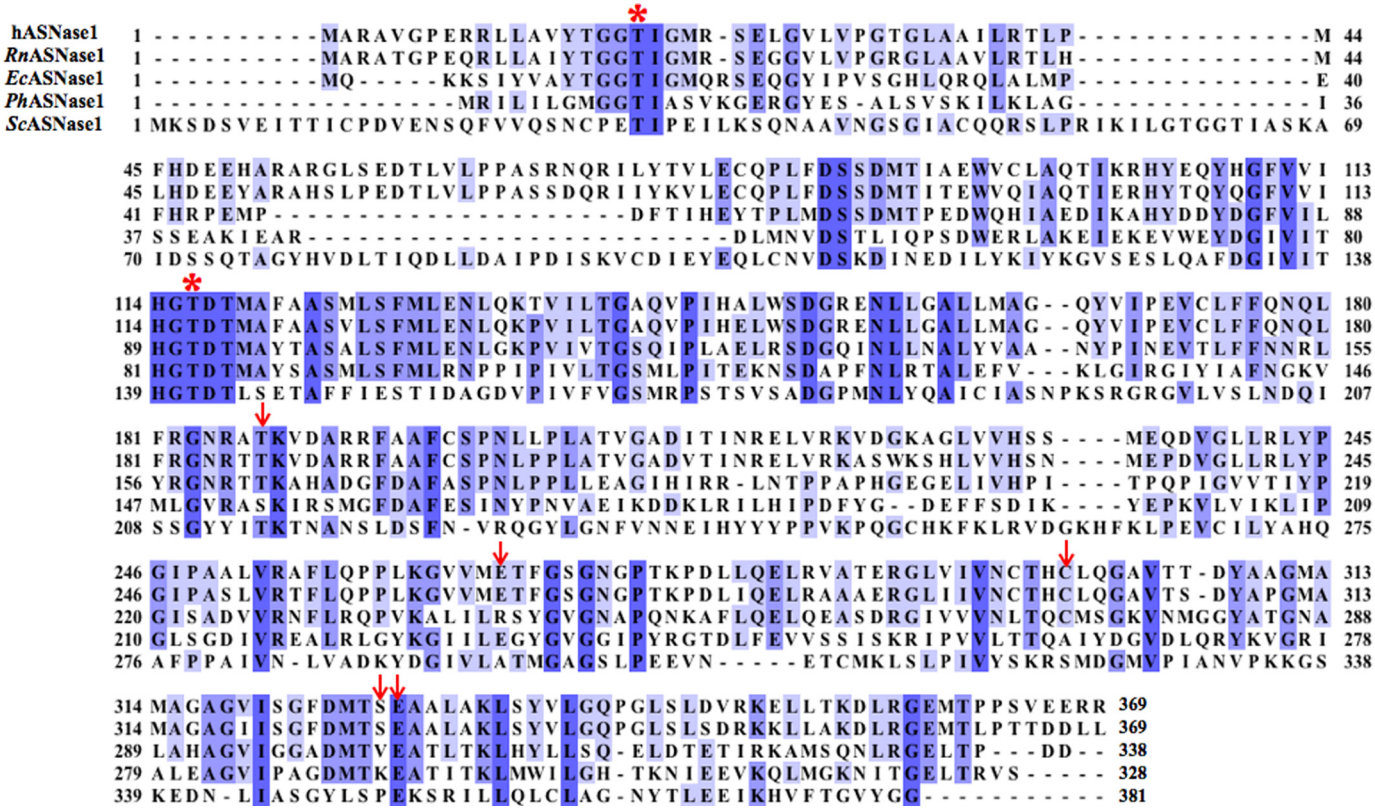

FIGURE 1. **Alignment of the amino acid sequences of hASNase1 (UniProt accession number Q86U10), *R. norvegicus* (UniProt accession number O88202), *E. coli* (UniProt accession number P0A962), *P. horikoshii* (UniProt accession number O57797), and *S. cerevisiae* (UniProt accession number P38986) L-asparaginases type I.** The displayed sequence of hASNase1 corresponds to truncation 4, which showed the best expression pattern of the four protein constructs produced in this work (see Fig. 2). *Asterisks* indicate the two threonine residues that are critical for L-asparaginase activity, and *red arrows* indicate residues that are located close to the allosteric sites. The alignment was performed using ClustalW (67), and the graph was generated using JalView (68). *Blue* shading indicates highly conserved amino acid residues.

ing their separation upon exhaustive washing (Fig. 3). It is worth mentioning that the bound GroEL did not affect the activity of hASNase1 because activity measurements on both enzyme preparations (with and without bound GroEL) yielded similar kinetic constants. We emphasize that all hASNase1 variants produced in this work were expressed at levels similar to the wild-type enzyme and showed no aggregation or precipitation tendency at any purification step. GroEL contamination was present during purification of all mutant enzymes as well.

Size exclusion chromatography experiments allowed us not only to obtain a highly pure protein as evidenced by SDS-PAGE analysis (Fig. 3) but also to gain insight into the oligomeric state of hASNase1. Strikingly, when we first analyzed native hASNase1, we observed that the enzyme (~3 μM) was running as a monomer (molecular mass, ~40 kDa) on a Superdex 200 gel filtration column (Fig. 4*C*). As the shift between oligomeric states of enzymes can be drastically influenced by their substrates and/or other interacting partners (45, 46), we decided to perform gel filtration analysis in the presence of the substrate of hASNase1. Interestingly, with 20 mM L-Asn in the running buffer, we witnessed a slightly shifted shoulder peak of the previously observed chromatographic peak assigned to the 40-kDa hASNase1 monomer, indicative of a higher molecular weight species, although the monomer remained the predominant form (Fig. 4*D*). This finding suggested that L-Asn could trigger the association of monomeric hASNase1 molecules and consequently induce the formation of dimers and even tetramers, which are the characteristic molecular species reported for *Ec*ASNase1 (25) as we confirmed in the present study (Fig. 4*B*). However, at enzymatic assay conditions, hASNase1 (~0.5 μM) is expected to be monomeric because this concentration is 6-fold lower than the concentration of the eluted monomeric protein shown in Fig. 4 (0.5 mg of enzyme loaded on the gel filtration column eluted in a final volume of ~4 ml of buffer, *i.e.* ~3 μM final concentration of the enzyme).

The hASNase1 Enzyme Shows Non-Michaelis-Menten Kinetics for L-Asn Hydrolysis Similar to Its E. coli Homolog but Lacks Lysophospholipase Activity—The N-terminal domain of human 60-kDa lysophospholipase, which we have designated as hASNase1, shares 47% sequence identity with *E. coli* cytoplasmic L-asparaginase (encoded by the *ansA* gene; *Ec*ASNase1). The crystal structure of *Ec*ASNase1 has been reported recently (25), shedding light on distinct structural features associated with L-Asn binding to the catalytic site and to the site responsible for allosteric regulation. Based on this structure, we modeled the hASNase1 structure using the Phyre program. Fig. 5 shows the active and the allosteric sites in the predicted hASNase1 structure overlaid by the homologous regions of *Ec*ASNase1. Residues critical for catalysis in the *E. coli* enzyme, such as Thr^{14}, Thr^{91}, Asp^{92}, and Lys^{163}, overlay with high accuracy with those of hASNase1, which has identical residues at these positions (Thr^{19}, Thr^{116}, Asp^{117}, and Lys^{188}) (Fig. 5*A*). Importantly, resi-

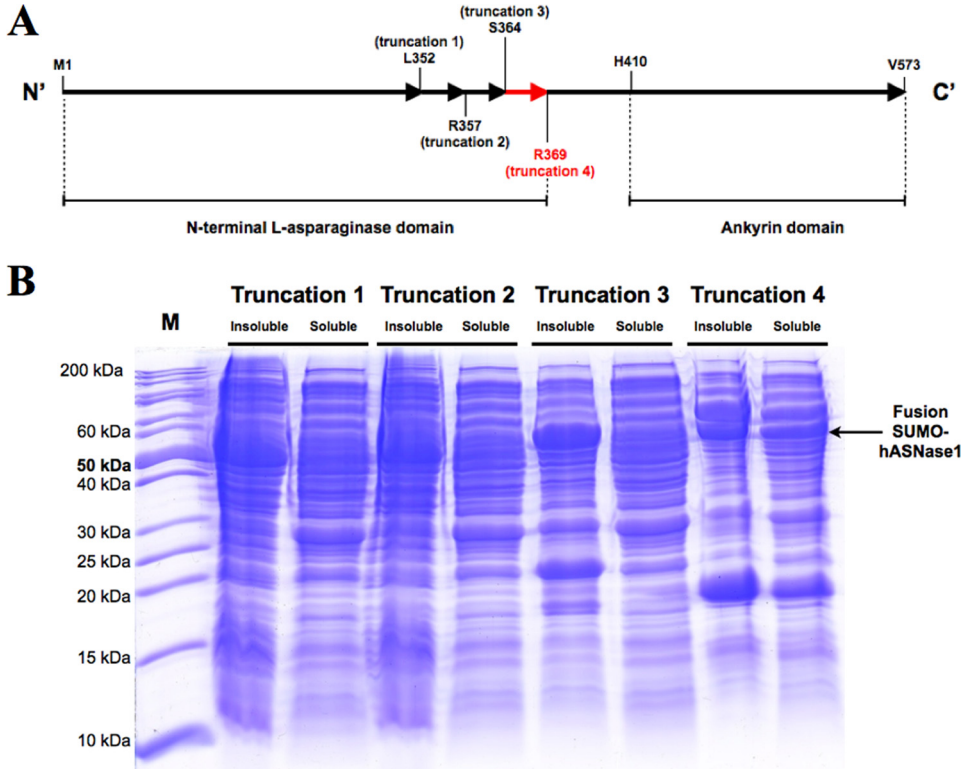

FIGURE 2. *A*, schematic representation of the full-length 60-kDa human lysophospholipase (Met[1]–Val[573]). Shown are the four different truncations that were generated and tested for protein solubility and L-asparaginase activity. Residues Leu[352], Arg[357], Ser[364], and Arg[369] indicate the last amino acid of the respective truncations. *Red* labeling indicates truncation 4 of the hASNase1 domain, which showed the best solubility and activity. Downstream of the L-asparaginase domain, the sequence region from His[410] to Val[573] indicates the putative ankyrin domains as also predicted in the rat homolog (23). *B*, SDS-PAGE analysis of all four expressed truncations of hASNase1. Insoluble and soluble fractions are included for each preparation. The *arrow* indicates the fusion SUMO-hASNase1 of truncation 4, which resulted in the production of soluble enzyme. The predicted molecular masses for each truncation as a fusion with SUMO are as follows: truncation 1, 50.5 kDa; truncation 2, 51.2 kDa; truncation 3, 51.9 kDa; and truncation 4, 52.5 kDa. *Lane M*, molecular mass markers.

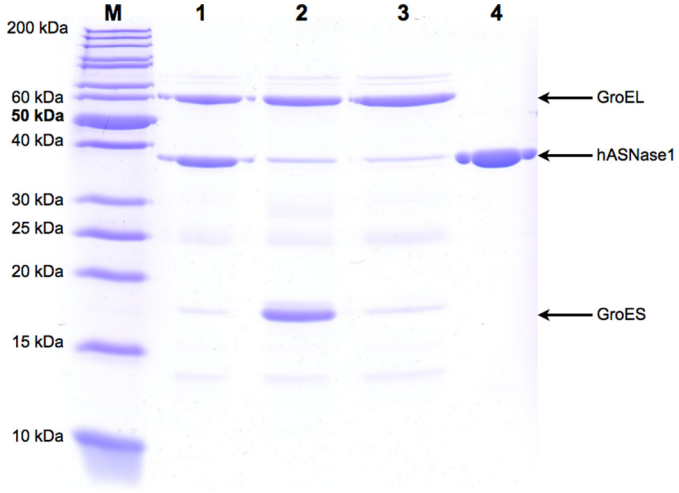

FIGURE 3. **Purification of hASNase1.** *Lane 1*, purified enzyme associated with GroEL; *lane 2*, removal of GroEL by complexation with externally added GroES in the Ni-NTA column; *lane 3*, washed GroEL fraction from DEAE anion exchange purification step; *lane 4*, final purity of hASNase1; *lane M*, molecular mass markers.

dues Thr[14] and Thr[91] of the bacterial enzyme are considered to be the primary nucleophiles for the attack on the substrate L-asparagine (25). The presence of threonine residues at equivalent positions in the human enzyme is in favor of the view that the primary nucleophile in bacterial L-asparaginases (both cytoplasmic and periplasmic) is a threonine residue (47). This prompted us to investigate this assumption for hASNase1 by mutagenesis studies. Indeed, when point mutants T19A and T116A of hASNase1 were assayed, no L-asparaginase activity was detected (Table 1), thus indicating the critical catalytic role of these threonine residues in hASNase1.

Steady-state kinetic characterization of wild-type hASNase1 using L-Asn as substrate (there was no detectable L-glutaminase activity) revealed that the enzyme did not follow Michaelis-Menten kinetics. Instead, it exhibited a pronounced sigmoidal kinetic behavior, which is a hallmark of allosteric enzymes. The kinetic data were fitted using the Hill equation (Equation 1 under "Experimental Procedures") from which we estimated a Hill coefficient (n_H) of 3.9 and an $S_{0.5}$ value of 11.5 mM (Fig. 6). The modeled structure of the allosteric site is shown in Fig. 5*B* in direct comparison with that of *Ec*ASNase1. Significant differences between the two allosteric sites are seen in two key residues that directly interact with the substrate L-Asn: Glu[266] and Ser[327] in hASNase1 as opposed to Arg[240] and Val[302] in the bacterial enzyme. Aiming at further characterization of the allosteric sites of both enzymes, we generated a series of mutants and expressed, purified, and tested them for catalytic activity. Strikingly, hASNase1 tolerated none of the mutations introduced in the predicted allosteric site as evidenced by the total lack of activity of the mutant enzymes (Table 1). Given the high structural homology between hASNase1 and *Ec*ASNase1, we reasoned that the mutation E266R could potentially lower the $S_{0.5}$ value of the human enzyme by mimicking the Arg[240]

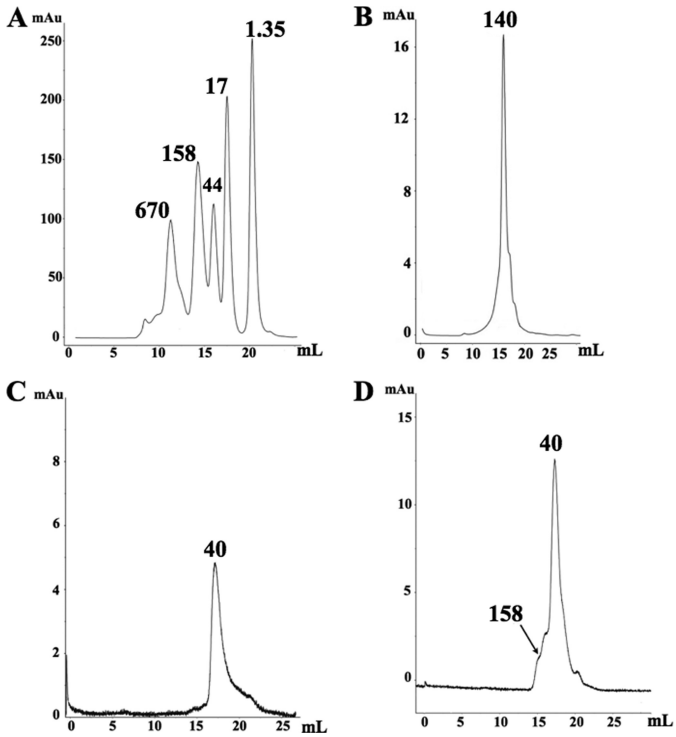

FIGURE 4. **Size exclusion chromatography profiles upon separation using Superdex 200 column (GE Healthcare).** *A*, standard gel filtration marker (Bio-Rad catalog number 151-1901). *B*, *Ec*ASNase1 chromatogram in 50 mM Tris-Cl, 100 mM NaCl, pH 8. *C*, profile of hASNase1 in the absence of L-Asn. Before sample loading, the column was equilibrated with 50 mM Tris-Cl, 100 mM NaCl, pH 8. *D*, hASNase1 in the presence of 20 mM L-Asn. The column was equilibrated with 50 mM Tris-Cl, 100 mM NaCl, 20 mM L-Asn, pH 8. In each case (*B*, *C*, and *D*), ~0.5 mg of enzyme was loaded on the column. *mAu*, milli-absorbance units.

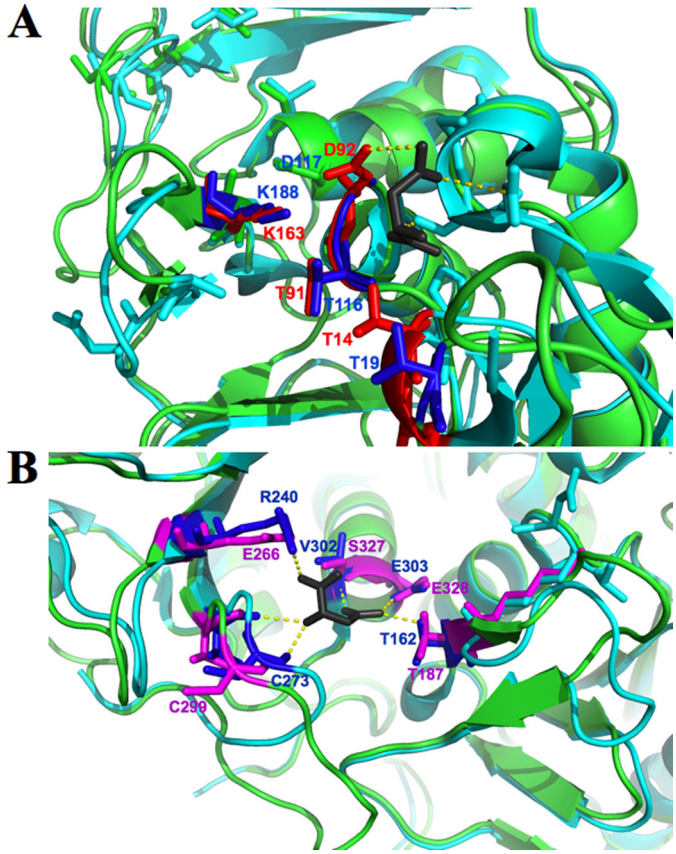

FIGURE 5. *A*, modeled active site of hASNase1 overlaid by the active site of *Ec*ASNase1. *Red* highlights amino acids that are critical for activity of bacterial L-asparaginases: the catalytic triad formed by residues Thr[91], Asp[92], and Lys[163] that ensure proper orientation of the substrate L-Asn (*dark gray*) and Thr[14], which is responsible for subsequent nucleophilic attack (23, 69). *Blue* highlights the respective amino acids of hASNase1: Thr[116], Asp[117], Lys[188], and Thr[19]. *B*, modeled allosteric site of hASNase1 (*magenta* residues) overlaid by the *Ec*ASNase1 allosteric site (*blue* residues). Key differences in homologous sites of the human enzyme are residues Glu[266] *versus* Arg[240] and Ser[327] *versus* Val[302]. Other residues of the allosteric sites of the two enzymes are highly similar. Also shown is an L-Asn molecule (*dark gray*), which interacts with allosteric site residues. The interactions between L-Asn and the human enzyme were predicted based on the structure of the bacterial enzyme (Protein Data Bank code 2HIM).

site of the bacterial homolog. However, this mutation totally inactivated hASNase1. Other mutations introduced around the putative allosteric site of hASNase1, such as E266S, C299S, T187S, and T187A, also abolished activity (Table 1). Unlike the human enzyme, the *E. coli* enzyme tolerated mutations of its allosteric site. Mutation R240E resulted in an ~5-fold increase of $S_{0.5}$ and 2-fold increase of k_{cat} while simultaneously lowering the Hill coefficient n_H from 3.55 to 1.9. The C273S mutation increased even further the $S_{0.5}$ value (7-fold with respect to wild type), whereas the n_H value slightly decreased (Fig. 6). All kinetic data of wild-type hASNase1 and *Ec*ASNase1 as well as of mutants generated in this work are summarized in Table 1. Taken together, these results suggest that despite the high similarity of sites predicted to be critical for their activities these two enzymes display different degrees of tolerance toward mutations of residues at these sites.

We additionally tested for potential hydrolysis of palmitoyl-lysoPC and lysoPI by hASNase1 and *Ec*ASNase1. We chose these two substrates because the rat 60-kDa lysophospholipase has been reported to hydrolyze palmitoyl-lysoPC (23), whereas lysoPI could serve as a substrate for the human homolog (24). However, we were unable to detect any activity of either hASNase1 or *Ec*ASNase1 using these two substrates under conditions where the control enzyme phospholipase A_2 hydrolyzed L-α-phosphatidylcholine. The rate of the fluorescence decrease in the ADIFAB assay was the same for the blank (ADIFAB plus substrate without enzyme) and the sample (ADIFAB plus sub-

TABLE 1

Kinetic data on wild-type and mutants of hASNase1 and *Ec*ASNase1

Steady-state kinetic analysis was performed by applying a continuous NADH-dependent assay (30). Enzyme concentrations were ~0.5 μM in a final volume of 1 ml of 50 mM Tris-Cl, 100 mM NaCl, pH 8 at 37 °C; the tested substrate concentrations covered the range of 0–10K_m. Parameters were calculated from non-linear regression of a *V*/*E* *versus* [L-Asn] plot using the software SoftZymics (Igor Pro, Wavemetrics). ND, non-detectable; the limit of detection for the applied assays in the present study is 0.5 μM of ammonia produced in a 1-ml reaction volume. Data are shown as mean values ±S.D. of triplicate measurements.

Enzyme	k_{cat}	$S_{0.5}$	n_H
	s^{-1}	mM	
Wild-type hASNase1	6.7 ± 0.2	11.5 ± 0.8	3.9 ± 0.2
hASNase1 T19A	ND	ND	
hASNase1 T116A	ND	ND	
hASNase1 E266R	ND	ND	
hASNase1 E266S	ND	ND	
hASNase1 T187A	ND	ND	
hASNase1 T187S	ND	ND	
hASNase1 C299S	ND	ND	
Wild-type *Ec*ASNase1	7.4 ± 0.3	0.40 ± 0.05	3.5 ± 0.3
*Ec*ASNase1 R240E	14.5 ± 0.5	1.8 ± 0.2	1.9 ± 0.2
*Ec*ASNase1 C273S	16.8 ± 0.4	2.8 ± 0.3	2.7 ± 0.2

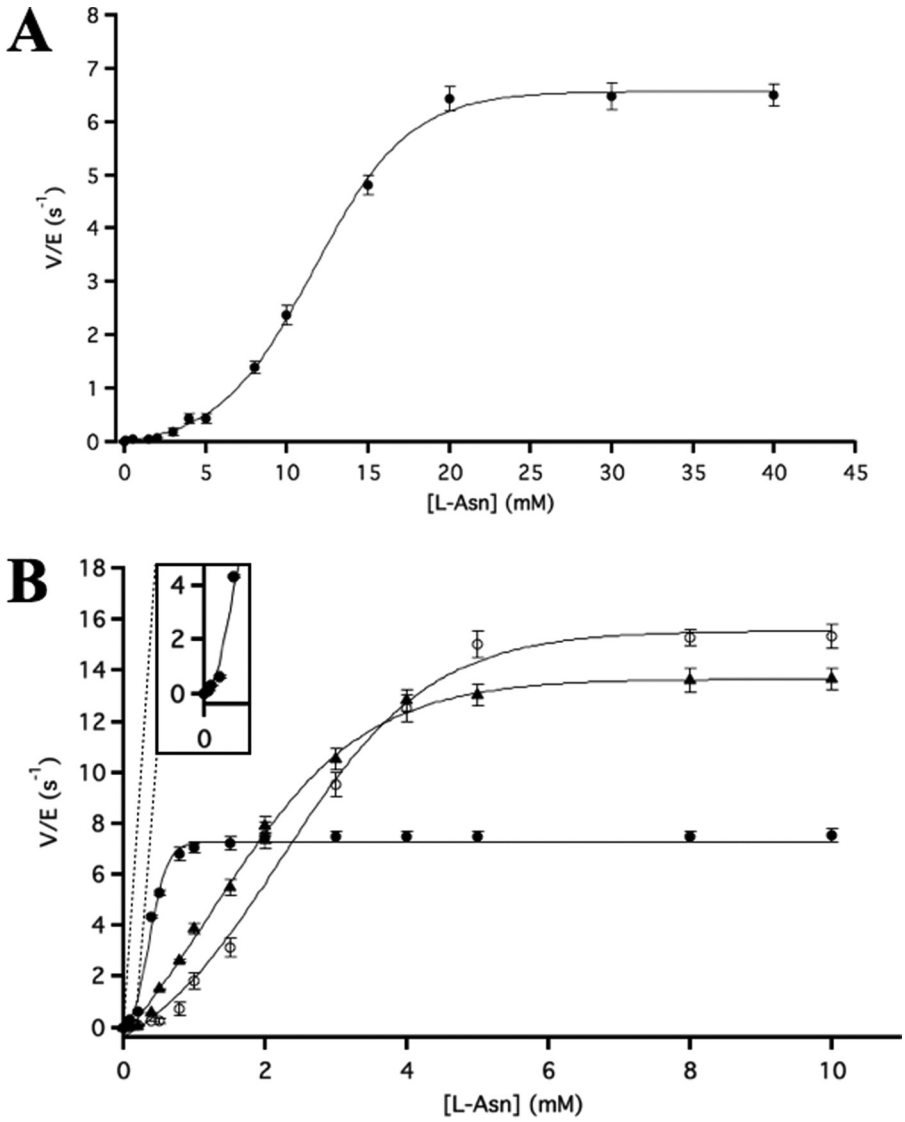

FIGURE 6. **L-Asparaginase activities as a function of substrate concentrations of hASNase1 and *Ec*ASNase1.** *A*, *V/E versus* [L-Asn] plot for wild-type hASNase1. Steady-state turnover rates (s^{-1}) are expressed as a function of the substrate concentration. Data points are represented as means ± S.D. of triplicate sample measurements. *B*, *V/E versus* [L-Asn] plots for C273S (○) and R240E (▲) mutants and wild type (●) *Ec*ASNase1. The *inset* shows a zoomed frame of the plot at low substrate concentrations for wild-type *Ec*ASNase1. Data points are mean values ±S.D. of triplicate measurements. All steady-state kinetic curves resulted from non-linear regression analysis using the Hill equation (Equation 1 under "Experimental Procedures") in SoftZymics software (Igor Pro, Wavemetrics). *Error bars* represent S.D.

strate and enzyme) and accounted for ~10 arbitrary fluorescence units/min (data available upon request). This background activity is in line with another study (31), which also reported a constant slight fluorescence signal decrease in the absence of enzyme. In conclusion, our results demonstrate that the N-terminal domain of the 60-kDa full-length human lysophospholipase can exist as a distinct folding unit that resembles the bacterial-type I L-asparaginases, lacking the capacity to hydrolyze substrates other than L-Asn.

Fluorescence Labeling of hASNase1—Cysteine labeling allowed us to investigate the presence of an L-Asn binding site distinct from the catalytic site in the monomer. This additional binding site could play the role of an allosteric site of hASNase1, and its existence is supported not only by the sigmoidal kinetic behavior of enzyme described in the previous paragraph but also by our results obtained from substrate titration to a fluorescence-labeled, catalytically inactive version of the protein. Binding of the substrate L-Asn to the putative allosteric site was monitored by fluorescence signal changes of the Atto dye-labeled enzyme. The dye was covalently attached to cysteine residue Cys^{299}, which according to the structural model built on the *E. coli* enzyme directly interacts with L-Asn bound to the allosteric site (Fig. 5*B*). The labeling of hASNase1 was confirmed by SDS-PAGE analysis as shown in Fig. 7 based on the observation that labeled proteins migrate more slowly than the unlabeled species (34). Fig. 8 shows a pronounced fluorescence signal decrease upon incubation of the catalytically inactive T19A mutant of hASNase1 with L-Asn in the concentration range of 0.1–40 mM. We did not label the wild-type enzyme because upon titration of L-Asn notably at high concentrations it would hydrolyze the substrate without allowing us to solely evaluate binding phenomena (the T19A mutant is assumed to maintain intact its allosteric site similarly to the wild-type enzyme). From the resulting binding curve, we estimated a K_d

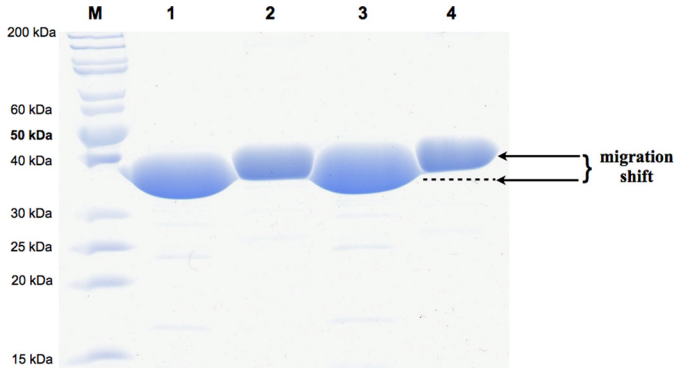

FIGURE 7. **SDS-PAGE analysis of unlabeled and labeled T19A and C299S mutants.** *Lane 1*, unlabeled T19A; *lane 2*, labeled T19A; *lane 3*, unlabeled C299S; *lane 4*, labeled C299S; *lane M*, molecular mass markers. The electrophoretic pattern clearly shows the migration difference between the labeled and unlabeled enzyme species.

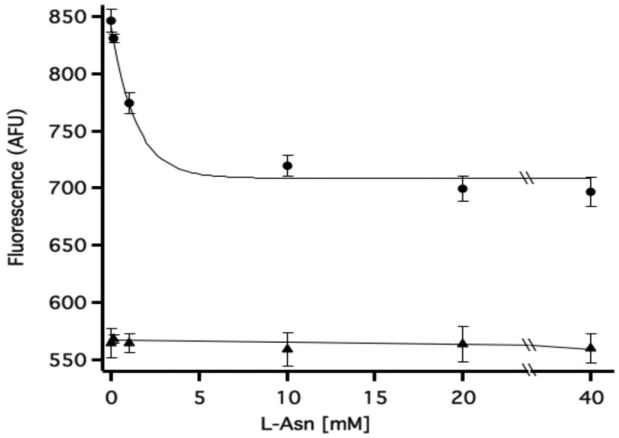

FIGURE 8. **Plot of fluorescence signal change of Atto 465-labeled T19A and C299S hASNase1 mutants as a function of L-Asn concentration.** Shown are the fluorescence signal decreases in the case of T19A indicating an induced conformational change upon binding of L-Asn to either the allosteric or the active site. In contrast, the C299S mutant, which is not labeled at the putative allosteric site, showed no signal changes upon L-Asn titration; constant background fluorescence results from labeling of other cysteines. The saturation binding curve for the T19A mutant was fitted to a hyperbolic function (Equation 2 in text) as described under "Experimental Procedures." In the case of C299S, where no fluorescence change was observed, the points were fitted to a *straight line*. *Error bars* represent S.D. *AFU*, arbitrary fluorescence units.

of ~1 mM, which is about 10-fold lower than the $S_{0.5}$ (~11 mM). Unlike T19A, the C299S mutant, which served as a negative control for labeling with the Atto dye, yielding a constant background fluorescence (due to labeling of other cysteines), showed no fluorescence signal changes upon incubation with L-Asn. This indicates that signal changes observed for T19A can be attributed to direct interaction of the substrate L-Asn with either Cys^{299} or other neighboring residues located within the allosteric cavity. Conversely, we cannot exclude potential interactions between L-Asn and the active site residues leading to conformational alterations that are transmitted to the allosteric site and reflected by fluorescence signal changes. Incubation of labeled enzyme with aspartate induced no fluorescence signal change (data not shown).

Thermodynamic Characterization of hASNase1 and EcASNase1—The free energy difference ΔG_{H2O} of folded and unfolded states, which is a measure of protein stability, was

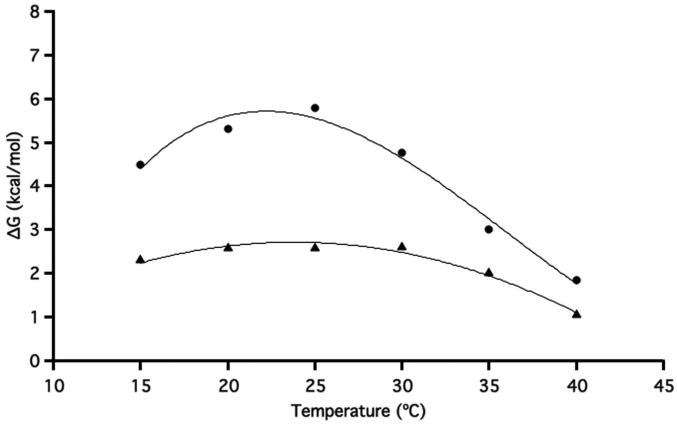

FIGURE 9. **Temperature dependence of free energy change during unfolding of human and bacterial ASNase1.** Shown is a plot of ΔG_{H2O} as obtained at various temperatures *versus* the respective temperatures for wild-type hASNase1 (▲) and *Ec*ASNase1 (●). Data were fitted to the Gibbs-Helmholtz equation (Equation 3 in text) after determining T_m and ΔH_m by thermal denaturation experiments (see "Experimental Procedures"). The standard deviation for ΔG_{H2O} (free energy change at zero concentration of urea), evaluated from three independent determinations on the wild-type enzymes at 25 °C, was found to be 0.3 kcal/mol.

TABLE 2

Thermodynamic parameters for wild-type hASNase1 and EcASNase1

The ΔC_p values were calculated using the Gibbs-Helmholtz equation (see text) upon plotting the experimentally determined $\Delta G(T)$, T_m, ΔS_m, and ΔH_m values. ΔS_m, T_m, and ΔH_m were determined from linear regression analysis of the thermal denaturation of either enzyme. Parameters are represented as means ± S.D. of three measurements.

Enzyme	ΔC_p	T_m	ΔH_m	ΔS_m
	kcal/mol × K	*°C*	*kcal/mol*	*cal/mol/K*
hASNase1	5.47 ± 0.20	58.40 ± 0.60	104.2 ± 1.5	314 ± 2
*Ec*ASNase1	3.10 ± 0.15	59.50 ± 0.45	89.7 ± 0.9	270 ± 1.5

determined for both enzymes from urea denaturation experiments at different temperatures (37). Non-linear regression analysis was applied to the experimentally obtained ΔG_{H2O} values using the Gibbs-Helmholtz equation as a function of temperature, which allows the calculation of the ΔC_p parameter (48). Fig. 9 shows the stability curves for both enzymes studied in this work for direct comparison of their characteristic features under identical conditions. At 25 °C, the bacterial enzyme has a 2-fold higher ΔG_{H2O} in comparison with the human enzyme, although this difference appears to decline at higher temperatures (35 and 40 °C) as has also been observed in other proteins (49). Table 2 summarizes thermodynamic parameters obtained for hASNase1 and *Ec*ASNase1. Interestingly, the predicted ΔC_p values are considerably different for the two enzymes, possibly pointing to variations in the surface area that is exposed upon denaturation (50) and distinct mechanisms of enthalpy and entropy changes occurring upon unfolding (51). The two enzymes exhibited similar melting temperatures T_m with hASNase1 showing higher ΔH_m and ΔS_m values, indicating higher enthalpy changes upon unfolding and a higher degree of disorder as compared with the *E. coli* enzyme (52).

Differential Scanning Fluorometry of hASNase1—To analyze whether allosteric and active site mutations influenced the thermal stability of hASNase1, several of these hASNase1 mutants were studied by differential scanning fluorometry. The melting curves were all monophasic (Fig. 10). The melting tem-

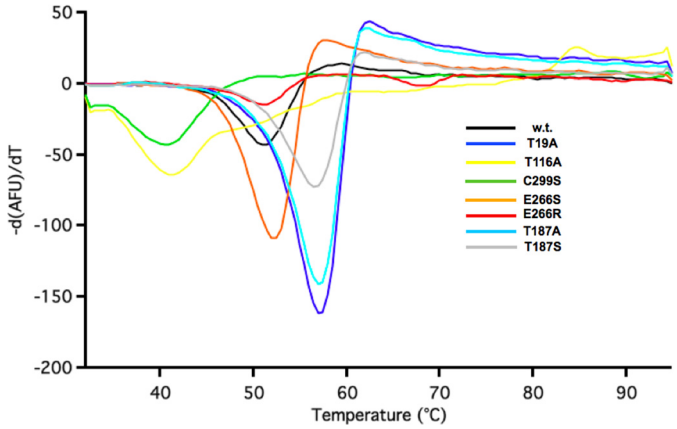

FIGURE 10. **Melting curves for wild-type and mutant hASNase1 as determined by differential scanning fluorometry.** Melting temperatures were calculated by plotting the first derivative d(AFU)/d*T* (where AFU represents arbitrary fluorescence units) of the raw data as a function of the temperature range tested (see "Experimental Procedures").

TABLE 3

Melting temperatures of wild-type and mutant hASNase1 as determined by differential scanning fluorometry

Samples of 2 μM highly purified enzyme solution were mixed with a 10% (v/v) final concentration of SYPRO Orange in a final volume of 20 μl in a 96-well plate. Enzyme melting experiments were performed using a CFX96 RT-PCR machine (Bio-Rad) and the following settings: 2-min prewarming step at 30 °C and subsequent gradient between 31 and 95 °C with 1 °C/min increments. SYPRO Orange fluorescence was monitored using FAM excitation (492 nm) and ROX emission (610 nm) filters. Melting temperatures (T_m) were calculated by plotting the first derivative d(AFU)/d*T* (where AFU represents arbitrary fluorescence units) of the raw data as a function of temperature increase (40).

Enzyme	T_m
	°C
Wild-type hASNase1	51.3
T19A	58.1
T116A	41
C299S	40
E266S	52.5
E266R	51
T187A	57.9
T187S	57.6

perature (T_m) values are summarized in Table 3. Our results suggest that three point mutations (T19A, T187A, and T187S) had a significant stabilizing effect on the enzyme. In contrast, mutations T116A and C299S considerably lowered protein stability as compared with wild type, whereas the two mutations (E266S and E266R) introduced at the allosteric site Glu^{266} had almost no effect on the stability of hASNase1.

Dependence of hASNase1 Activity on pH and Metal Ions—The optimum activity of hASNase1 was investigated in the pH range from 2.5 to 10. Fig. 11*A* shows that the enzyme exhibited the highest activity in a relatively narrow alkaline pH range as evidenced by a sharp increase from pH 7 to 8 followed by an immediate decline from pH 8.5 to 10. In addition, the pH dependence for stability of the enzyme showed a maximum peak at pH 8 (Fig. 11*B*). These results suggest that protonation of certain residues that are involved in catalysis might partially impair the activity of hASNase1. Furthermore, certain divalent metal ions, such as Cd^{2+} and Cu^{2+} at 1 mM, totally inhibited hASNase1 activity, whereas DTT, Co^{2+}, Ca^{2+}, Ni^{2+}, Mg^{2+}, Mn^{2+}, Fe^{2+}, and Li^{+} only weakly influenced the hydrolysis of L-Asn. Such metal-selective inhibition by Cd^{2+} and Cu^{2+} possibly indicates an interaction between these metal ions and a

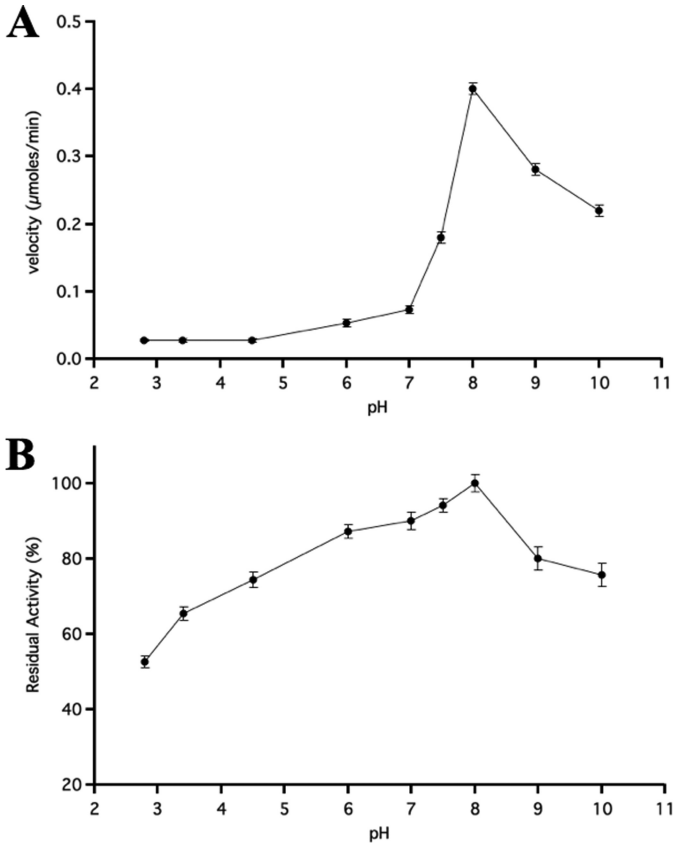

FIGURE 11. **Effect of pH on hASNase1 activity (*A*) and stability (*B*).** Buffers used were: sodium acetate (pH 3–5), sodium phosphate (pH 6–7), Tris-Cl (pH 7–8.5), and CAPSO (pH 9–10), all at 50 mM concentration in 100 mM NaCl. Enzymatic activities were determined as described under "Experimental Procedures" applying the Nesslerization assay for determining ammonia generated by L-asparagine hydrolysis. *Error bars* represent S.D.

TABLE 4

Effect of different salts, EDTA, and DTT on the activity of hASNase1

Purified hASNase1 (0.1 mg/ml) in 1 ml was preincubated with a final concentration of 1 mM each of several divalent metal ions, EDTA, and DTT for 3 h at 4 °C. Subsequently, aliquots were tested for residual L-asparaginase activity by the Nesslerization method (29). Data are shown as mean values ±S.D. of triplicate measurements.

Compound (1 mM)	Remaining activity
	%
EDTA	100 ± 0.6
DTT	64 ± 4.1
$NiSO_4$	90 ± 4.0
$CoCl_2$	68 ± 4.0
$CaCl_2$	84 ± 3.5
$MgCl_2$	89 ± 4.0
$CdCl_2$	0
$MnSO_4$	89 ± 1.8
Fe_2SO_4	73 ± 2.8
LiCl	64 ± 3.8
$CuCl_2$	0

thiol group pivotal for activity (53). A candidate might be the Cys^{299} residue, which is located at the allosteric site of the enzyme and plays an important role in L-Asn binding. In addition, EDTA at concentrations up to 1 mM had no noticeable negative effect on the activity of hASNase1 (Table 4).

DISCUSSION

The present study focuses on the biochemical analysis of the N-terminal domain of a human 60-kDa protein designated as lysophospholipase. The full-length version of this two-do-

main protein has been only poorly characterized in one report (24). Our primary motivation to produce and functionally characterize the N-terminal domain of this protein, which structurally and according to its catalytic *in vitro* properties significantly resembles *E. coli* cytoplasmic L-asparaginase (*ansA*; *Ec*ASNase1), originated from our previous work on human enzymes that possess L-asparaginase activity (10, 19, 21). The discovery, molecular engineering, and *in vitro* evolution of catalytically efficient human L-asparaginases are thought to lay the basis for the replacement of bacterial L-asparaginases presently used as antileukemia therapeutics despite adverse side effects mainly attributed to their bacterial origins (54).

An early study on the rat 60-kDa lysophospholipase (23) assigned three distinct activities to this enzyme acting as lysophospholipase, L-asparaginase, and acetylhydrolase on the platelet-activating factor. Several years later, a report on the human 60-kDa lysophospholipase (24) revealed a specific role of this enzyme as an interacting partner of the serum- and glucocorticoid-induced serine/threonine protein kinase Sgk1, an enzyme involved in various cell proliferation pathways. In contrast to its rat homolog, the human enzyme was not reported to bear L-asparaginase activity (24). However, in both these studies, the distinct enzymatic activities were determined only qualitatively using lysates from cells overexpressing the respective genes rather than purified enzyme preparations.

Here, we show that the N-terminal L-asparaginase domain (residues 1–369) of the 573-residue human protein, that we termed hASNase1, can be produced in soluble form in *E. coli*. This protein showed L-asparaginase activity with a maximum catalytic rate of about 7 s^{-1}, which is very similar to that of *Ec*ASNase1, implying that this N-terminal domain forms a stable and functional folding unit in the absence of the C-terminal putative ankyrin repeat domain. Kinetic and mutational characterization of hASNase1 revealed strong positive allosteric modulation in the velocity *versus* substrate plot similar to its *E. coli* homolog. To validate our experimental strategy for characterizing this human counterpart of the cytosolic *E. coli* L-asparaginase, we also recombinantly produced the bacterial protein to directly compare the two enzymes under identical assay conditions. Our kinetic data obtained on the bacterial enzyme are consistent with a previous study that centered on its structural analysis and allosteric regulation (25).

Given the pronounced sigmoidal kinetic behavior that we observed in steady-state kinetics of L-asparagine hydrolysis, we hypothesized that hASNase1 possesses an allosteric site that could act as "sensor" for the presence of substrate. Our dye labeling approach targeting the Cys^{299} residue indicated fluorescence signal changes upon binding of L-Asn, thus strengthening the idea of the existence of such an allosteric site that can be regulated by the substrate L-Asn. In the absence of information on the three-dimensional structure of hASNase1, which could provide more detailed insight into the catalytic mechanism and allosteric regulation of the enzyme, we referred to a structural homology-model based on the *Ec*ASNase1 crystal structure, which allowed us to define the active site and an allosteric site of the human enzyme. The $S_{0.5}$ value of 11.5 mM determined for hASNase1 is about 10-fold higher than that reported for the *E. coli* enzyme, raising questions about the physiological role of the full-length protein and its N-terminal domain displaying L-asparaginase activity as shown in this work. The relatively high $S_{0.5}$ value determined for the human enzyme falls well within the range of free concentrations of intracellular amino acids (>10 mM), including L-Asn, reported for mammalian cells (55, 56), thus making the enzyme operate efficiently, particularly at elevated substrate concentrations.

The homo-oligomeric *Ec*ASNase1 displays sigmoidal kinetics, which can be explained by positive cooperativity induced by the substrate L-Asn. In contrast, hASNase1, which shows non-Michaelis-Menten kinetics similar to its *E. coli* homolog, is monomeric under the conditions of activity measurements. In fact, a number of monomeric enzymes exhibiting allosteric behavior have been reported of which the most thoroughly characterized is human glucokinase (57, 58). However, glucokinase (also called hexokinase IV), unlike L-asparaginase, is a two-substrate (ATP plus glucose) enzyme and displays a moderate degree of allostery (59). However, monomeric enzymes with single binding sites, like hASNase1, can also show allostery (60). Two basic models have been put forward aiming at the mechanistic explanation of monomeric allostery: the mnemonic model (61) and the ligand-induced slow transition model (62). Both models assume the existence of two different enzyme conformations that are characterized by distinct affinities for the substrate (low and high affinity states). Depending on the substrate concentration, certain conformational changes may occur, thereby perturbing the equilibrium of the two states in favor of the high affinity state and an increased catalytic activity. Based on the observed sigmoidal kinetic behavior and the monomeric state of hASNase1, it appears plausible to assume that this is another example of a monomeric enzyme exhibiting positive allosteric regulation. Importantly, given the fact that L-Asn plays a dual role of being both substrate and regulator of hASNase1, L-Asn can be considered as a homotropic allosteric effector of this enzyme, adding to the steadily growing number of allosterically regulated proteins (63).

The role of the putative ankyrin repeat structure located in the C-terminal part of the full-length protein remains unknown at present. In numerous other proteins, ankyrin repeats were shown to mediate protein-protein interactions, and therefore, they may play crucial roles in cellular signaling events (64–66). The study of the kinetics of the full-length 60-kDa human lysophospholipase could provide information on the potential influence of the ankyrin repeat domain on the L-asparaginase activity predicted to reside in the N-terminal part. On the other hand, when we tested palmitoyl-lysoPC and lysoPI as potential substrates for hASNase1, we detected no lipase activity. Our biochemical data clearly support the view that the N-terminal domain bears L-asparaginase activity that exhibits positive allosteric regulation by the substrate L-Asn. A particular characteristic of hASNase1 is its monomeric state in conjunction with its pronounced sigmoidal steady-state kinetics. We would like to emphasize that the distinct enzymatic activities assigned to rat and human 60-kDa lysophospholipases warrant further analyses at the cellular level to elucidate the physiological role of these two-domain proteins. Our studies on L-asparaginase activity inherent to the N-terminal domain of this 60-kDa protein expands the basis of our work aiming at the identification

and molecular engineering of enzymes of human origin (10, 21) that might become suitable for replacing bacterial enzymes as approved therapeutics in the treatment of leukemias.

Acknowledgments—We thank Henning Urlaub and his team for expert mass spectrometry analyses and protein identification, Ursula Welscher-Altschäffel for technical assistance, and Claudia Höbartner for helpful comments on the manuscript.

REFERENCES

1. Credali, A., García-Calderón, M., Dam, S., Perry, J., Díaz-Quintana, A., Parniske, M., Wang, T. L., Stougaard, J., Vega, J. M., and Márquez, A. J. (2013) The K^+-dependent asparaginase, NSE1, is crucial for plant growth and seed production in Lotus japonicus. *Plant Cell Physiol.* **54,** 107–118
2. Willis, R. C., and Woolfolk, C. A. (1975) L-Asparagine uptake in *Escherichia coli*. *J. Bacteriol.* **123,** 937–945
3. Michalska, K., and Jaskolski, M. (2006) Structural aspects of L-asparaginases, their friends and relations. *Acta Biochim. Pol.* **53,** 627–640
4. Hejazi, M., Piotukh, K., Mattow, J., Deutzmann, R., Volkmer-Engert, R., and Lockau, W. (2002) Isoaspartyl dipeptidase activity of plant-type asparaginases. *Biochem. J.* **364,** 129–136
5. Srikhanta, Y. N., Atack, J. M., Beacham, I. R., and Jennings, M. P. (2013) Distinct physiological roles for the two L-asparaginases isozymes of *Escherichia coli*. *Biochem. Biophys. Res. Commun.* **436,** 362–365
6. Stecher, A. L., de Deus, P. M., Polikarpov, I., and Abrahão-Neto, J. (1999) Stability of L-asparaginase: an enzyme used in leukemia treatment. *Pharm. Acta Helv.* **74,** 1–9
7. Duval, M., Suciu, S., Ferster, A., Rialland, X., Nelken, B., Lutz, P., Benoit, Y., Robert, A., Manel, A. M., Vilmer, E., Otten, J., and Philippe, N. (2002) Comparison of *Escherichia coli*-asparaginase with *Erwinia*-asparaginase in the treatment of childhood lymphoid malignancies: results of a randomized European Organization for Research and Treatment of Cancer-Children's Leukemia Group phase 3 trial. *Blood* **99,** 2734–2739
8. Asselin, B. L., Ryan, D., Frantz, C. N., Bernal, S. D., Leavitt, P., Sallan, S. E., and Cohen, H. J. (1989) *In vitro* and *in vivo* killing of acute lymphoblastic leukemia cells by L-asparaginase. *Cancer Res.* **49,** 4363–4368
9. Brannigan, J. A., Dodson, G., Duggleby, H. J., Moody, P. C., Smith, J. L., Tomchick, D. R., and Murzin, A. G. (1995) A protein catalytic framework with an N-terminal nucleophile is capable of self-activation. *Nature* **378,** 416–419
10. Karamitros, C. S., and Konrad, M. (2014) Bacterial co-expression of the α and β protomers of human L-asparaginase-3: achieving essential N-terminal exposure of a catalytically critical threonine located in the β-subunit. *Protein Expr. Purif.* **93,** 1–10
11. Borek, D., Michalska, K., Brzezinski, K., Kisiel, A., Podkowinski, J., Bonthron, D. T., Krowarsch, D., Otlewski, J., and Jaskolski, M. (2004) Expression, purification and catalytic activity of *Lupinus luteus* asparagine β-amidohydrolase and its *Escherichia coli* homolog. *Eur. J. Biochem.* **271,** 3215–3226
12. Guan, C., Liu, Y., Shao, Y., Cui, T., Liao, W., Ewel, A., Whitaker, R., and Paulus, H. (1998) Characterization and functional analysis of the cis-autoproteolysis active center of glycosylasparaginase. *J. Biol. Chem.* **273,** 9695–9702
13. Oinonen, C., Tikkanen, R., Rouvinen, J., and Peltonen, L. (1995) Three-dimensional structure of human lysosomal aspartylglucosaminidase. *Nat. Struct. Biol.* **2,** 1102–1108
14. Saito, S., Ohno, K., Sugawara K., Suzuki, T, Togawa, T., and Sakuraba, H. (2008) Structural basis for aspartylglucosaminuria. *Biochem. Biophys. Res. Commun.* **377,** 1168–1172
15. Cantor, J. R., Stone, E. M., Chantranupong, L., and Georgiou, G. (2009) The human asparaginase-like protein 1 hASRGL1 is an Ntn hydrolase with β-aspartyl peptidase activity. *Biochemistry* **48,** 11026–11031
16. Dieterich, D. C., Landwehr, M., Reissner, C., Smalla, K. H., Richter, K., Wolf, G., Böckers, T. M., Gundelfinger, E. D., and Kreutz, M. R. (2003) Gliap: a novel untypical L-asparaginase localized to rat brain astrocytes. *J. Neurochem.* **85,** 1117–1125
17. Weidle, U. H., Evtimova, V., Alberti, S., Guerra, E., Fersis, N., and Kaul, S. (2009) Cell growth stimulation by CRASH, an asparaginase-like protein overexpressed in human tumors and metastatic breast cancers. *Anticancer Res.* **29,** 951–963
18. Michalska, K., Brzezinski, K., and Jaskolski, M. (2005) Crystal structure of isoaspartyl aminopeptidase in complex with L-aspartate. *J. Biol. Chem.* **280,** 28484–28491
19. Nomme, J., Su, Y., Konrad, M., and Lavie, A. (2012) Structures of apo and product-bound human L-asparaginase: insights into the mechanism of auto-proteolysis and substrate hydrolysis. *Biochemistry* **51,** 6816–6826
20. Li, W., Cantor, J. R., Yogesha, S. D., Yang, S., Chantranupong, L., Liu, J. Q., Agnello, G., Georgiou, G., Stone, E. M., and Zhang, Y. (2012) Uncoupling intramolecular processing and substrate hydrolysis in the N-terminal nucleophile hydrolase hASRGL1 by circular permutation. *ACS Chem. Biol.* **7,** 1840–1847
21. Su, Y., Karamitros, C. S., Nomme, J., McSorley, T., Konrad, M., and Lavie, A. (2013) Free glycine accelerates the autoproteolytic activation of human asparaginase. *Chem. Biol.* **20,** 533–540
22. Lowenson, J. D., Kim, E., Young, S. G., and Clarke, S. (2001) Limited accumulation of damaged proteins in L-isoaspartyl (D-aspartyl) *O*-methyltransferase-deficient mice. *J. Biol. Chem.* **276,** 20695–20702
23. Sugimoto, H., Odani, S., and Yamashita, S. (1998) Cloning and expression of cDNA encoding rat liver 60-kDa lysophospholipase containing an asparaginase-like region and ankyrin repeat. *J. Biol. Chem.* **273,** 12536–12542
24. Menniti, M., Iuliano, R., Föller, M., Sopjani, M., Alesutan, I., Mariggiò, S., Nofziger, C., Perri, A. M., Amato, R., Blazer-Yost, B., Corda, D., Lang, F., and Perrotti, N. (2010) 60 kDa lysophospholipase, a new Sgk1 molecular partner involved in the regulation of ENaC. *Cell Physiol. Biochem.* **26,** 587–596
25. Yun, M. K., Nourse, A., White, S. W., Rock, C. O., and Heath R. J. (2007) Crystal structure and allosteric regulation of the cytoplasmic *Escherichia coli* L-asparaginase I. *J. Mol. Biol.* **369,** 794–811
26. Peroutka, R. J., 3rd, Orcutt, S. T., Strickler, J. E., and Butt, T. R. (2011) SUMO fusion technology for enhanced protein expression and purification in prokaryotes and eukaryotes. *Methods Mol. Biol.* **705,** 15–30
27. Bradford, M. M. (1976) A rapid and sensitive method for the quantitation of microgram quantities of protein utilizing the principle of protein-dye binding. *Anal. Biochem.* **72,** 248–254
28. Noble, J. E., and Bailey, M. J. A. (2009) in *Methods in Enzymology* (Burgess, R. R., and Deutscher, M. P., eds), pp. 73–95, Academic Press, Waltham, MA
29. Derst, C., Henseling, J., and Röhm, K. H., (1992) Probing the role of threonine and serine residues of *E.coli* asparaginase II by site-specific mutagenesis. *Protein Eng.* **5,** 785–789
30. Balcão, V. M., Mateo, C., Fernández-Lafuente, R., Malcata, F. X., and Guisán, J. M. (2001) Structural and functional stabilization of L-asparaginase via multisubunit immobilization onto highly activated supports. *Biotechnol. Prog.* **17,** 537–542
31. She, H. S., Garsetti, D. E., Steiner, M. R., Egan, R. W., and Clark, M. A. (1994) The substrate specificities of four different lysophospholipases as determined by a novel fluorescence assay. *Biochem. J.* **298,** 23–29
32. Kelley, L. A., and Sternberg, M. J. (2009) Protein structure prediction on the Web: a case study using the Phyre server. *Nat. Protoc.* **4,** 363–371
33. DeLano, D. W. (2002) *The PyMOL Molecular Graphics System*, Schrödinger, LLC, New York
34. Modesti, M. (2011) in *Methods in Molecular Biology* (Peterman, E. J. G., and Wuite, G. J. L., eds), pp. 101–120, Humana Press Inc., New York
35. Grimsley, G. R., Trevino, S. R., Thurlkill, R. L., and Scholtz, J. M. (2013) Determining the conformational stability of a protein from urea and thermal unfolding curves. *Curr. Protoc. Protein Sci.* **71,** 28.4.1–28.4.14
36. Shirley B. A. (1995) in *Methods in Molecular Biology* (Shirley, B. A., ed), pp. 177–190, Humana Press Inc., New York
37. Baskakov, I. V., and Bolen, D. W., (1999) The paradox between m values and ΔCp's for denaturation of ribonuclease T1 with disulfide bonds intact and broken. *Protein Sci.* **8,** 1314–1319
38. Vedadi, M., Niesen, F. H., Allali-Hassani, A., Fedorov, O. Y., Finerty, P. J., Jr., Wasney, G. A., Yeung, R., Arrowsmith, C., Ball, L. J., Berglund, H., Hui,

R., Marsden, B. D., Nordlund, P., Sundstrom, M., Weigelt, J., and Edwards, A. M. (2006) Chemical screening methods to identify ligands that promote protein stability, protein crystallization, and structure determination. *Proc. Natl. Acad. Sci. U.S.A.* **103,** 15835–15840
39. Matulis, D., Kranz, J. K., Salemme, F. R., and Todd, M. J. (2005) Thermodynamic stability of carbonic anhydrase: measurements of binding affinity and stoichiometry using ThermoFluor. *Biochemistry* **44,** 5258–5266
40. Boivin, S., Kozak, S., and Meijers, R. (2013) Optimization of protein purification and characterization using Thermofluor screens. *Protein Expr. Purif.* **91,** 192–206
41. Rial, D. V., and Ceccarelli, E. A. (2002) Removal of DnaK contamination during fusion protein purifications. *Protein Expr. Purif.* **25,** 503–507
42. Rohman, M., and Harrison-Lavoie, K. J. (2000) Separation of copurifying GroEL from glutathione-S-transferase fusion proteins. *Protein Expr. Purif.* **20,** 45–47
43. Calloni, G., Chen, T., Schermann, S. M., Chang, H. C., Genevaux, P., Agostini, F., Tartaglia, G. G., Hayer-Hartl, M., and Hartl, F. U. (2012) DnaK functions as a central hub in the *E.coli* chaperone network. *Cell Rep.* **1,** 251–264
44. Thain, A., Gaston, K., Jenkins, O., and Clarke, A. R. (1996) A method for the separation of GST fusion proteins from co-purifying GroEL. *Trends Genet.* **12,** 209–210
45. O'Brien, J. R., Schuller, D. J., Yang, V. S., Dillard, B. D., and Lanzilotta, W. N. (2003) Substrate-induced conformational changes in *Escherichia coli* taurine/α-ketoglutarate dioxygenase and insight into the oligomeric structure. *Biochemistry* **42,** 5547–5554
46. Ereño-Orbea, J., Majtan, T., Oyenarte, I., Kraus, J. P., and Martínez-Cruz, L. A. (2013) Structural basis of regulation and oligomerization of human cystathionine β-synthase, the central enzyme of transsulfuration. *Proc. Natl. Acad. Sci. U.S.A.* **110,** E3790–E3799
47. Swain, A. L., Jaskólski, M., Housset, D., Rao, J. K., and Wlodawer, A. (1993) Crystal structure of *Escherichia coli* L-asparaginase, an enzyme used in cancer therapy. *Proc. Natl. Acad. Sci. U.S.A.* **90,** 1474–1478
48. Talla-Singh, D., and Stites, W. E. (2008) Refinement of noncalorimetric determination of the change in heat capacity, ΔC_p, of protein unfolding and validation across a wide temperature range. *Proteins* **71,** 1607–1616
49. Pace, C. N., Grimsley, G. R., Thomas, S. T., and Makhatadze, G. I. (1999) Heat capacity change for ribonuclease A folding. *Protein Sci.* **8,** 1500–1504
50. Spolar, R. S., Livingstone, J. R., and Record, M. T., Jr. (1992) Use of liquid hydrocarbon and amide transfer data to estimate contributions to thermodynamic functions of protein folding from the removal of nonpolar and polar surface from water. *Biochemistry* **31,** 3947–3955
51. Greene, R. F., Jr., and Pace, C. N. (1974) Urea and guanidine hydrochloride denaturation of ribonuclease, lysozyme, α-chymotrypsin, and β-lactoglobulin. *J. Biol. Chem.* **249,** 5388–5393
52. Baryshnikova, E. N., Melnik, B. S., Finkelstein, A. V., Semisotnov, G. V., and Bychkova, V. E. (2005) Three-state protein folding: experimental determination of free-energy profile. *Protein Sci.* **14,** 2658–2667
53. Bandyopadhyay, D., Chatterjee, A. K., and Datta, A. G. (1997) Effect of cadmium, mercury and copper on partially purified hepatic flavokinase of rat. *Mol. Cell. Biochem.* **167,** 73–80
54. Pieters, R., Hunger, S. P., Boos, J., Rizzari, C., Silverman, L., Baruchel, A., Goekbuget, N., Schrappe, M., and Pui, C. H. (2011) L-Asparaginase treatment in acute lymphoblastic leukemia: a focus on *Erwinia* asparaginase. *Cancer* **117,** 238–249
55. Chaneton, B., Hillmann, P., Zheng, L., Martin, A. C., Maddocks, O. D., Chokkathukalam, A., Coyle, J. E., Jankevics, A., Holding, F. P., Vousden, K. H., Frezza, C., O'Reilly, M., and Gottlieb, E. (2012) Serine is a natural ligand and allosteric activator of pyruvate kinase M2. *Nature* **491,** 458–462
56. Hansen, H. A., and Emborg, C. (1994) Extra- and intracellular amino acid concentrations in continuous Chinese hamster ovary cell culture. *Appl. Microbiol. Biotechnol.* **41,** 560–564
57. Kamata, K., Mitsuya, M., Nishimura, T., Eiki, J., and Nagata, Y. (2004) Structural basis for allosteric regulation of the monomeric allosteric enzyme human glucokinase. *Structure* **12,** 429–438
58. Zhang, J., Li, C., Chen, K., Zhu, W., Shen, X., and Jiang, H. (2006) Conformational transition pathway in the allosteric process of human glucokinase. *Proc. Natl. Acad. Sci. U.S.A.* **103,** 13368–13373
59. Cárdenas, M. L. (2013) Michaelis and Menten and the long road to the discovery of cooperativity. *FEBS Lett.* **587,** 2767–2771
60. Porter, C. M., and Miller, B. G. (2012) Cooperativity in monomeric enzymes with single ligand-binding sites. *Bioorg. Chem.* **43,** 44–50
61. Ricard, J., Meunier, J. C., and Buc, J. (1974) Regulatory behavior of monomeric enzymes. 1. The mnemonical enzyme concept. *Eur. J. Biochem.* **49,** 195–208
62. Cárdenas, M. L., Rabajille, E., and Niemeyer, H. (1984) Suppression of kinetic cooperativity of hexokinase D (glucokinase) by competitive inhibitors. A slow transition model. *Eur. J. Biochem.* **145,** 163–171
63. Huang, Z., Mou, L., Shen, Q., Lu, S., Li, C., Liu, X., Wang, G., Li, S., Geng, L., Liu, Y., Wu, J., Chen, G., and Zhang, J. (2014) ASD v2.0: updated content and novel features focusing on allosteric regulation. *Nucleic Acids Res.* **42,** D510–D516
64. Li, J., Mahajan, A., and Tsai, M. D. (2006) Ankyrin repeat: a unique motif mediating protein-protein interactions. *Biochemistry* **45,** 15168–15178
65. Bennett, V., and Chen, L. (2001) Ankyrins and cellular targeting of diverse membrane proteins to physiological sites. *Curr. Opin. Cell Biol.* **13,** 61–67
66. Voronin, D. A., and Kiseleva, E. V. (2007) Functional role of proteins containing ankyrin repeats. *Tsitologiia* **49,** 989–999
67. Larkin, M. A., Blackshields, G., Brown, N. P., Chenna, R., McGettigan, P. A., McWilliam, H., Valentin, F., Wallace, I. M., Wilm, A., Lopez, R., Thompson, J. D., Gibson, T. J., and Higgins, D. G. (2007) Clustal W and Clustal X version 2.0. *Bioinformatics* **23,** 2947–2948
68. Waterhouse, A. M., Procter, J. B., Martin, D. M., Clamp, M., and Barton, G. J. (2009) Jalview Version 2: a multiple sequence alignment editor and analysis workbench. *Bioinformatics* **25,** 1189–1191
69. Lubkowski, J., Palm, G. J., Gilliland, G. L., Derst, C., Röhm, K. H., and Wlodawer, A. (1996) Crystal structure and amino acid sequence of *Wolinella succinogenes* L-asparaginase. *Eur. J. Biochem.* **241,** 201–207